Wind turbine noise modeling: prediction of amplitude modulation and influence of atmospheric conditions

Yuan Tian, Benjamin Cotté, Antoine Chaigne

Wind turbine noise modeling: prediction of amplitude modulation and influence of atmospheric conditions

Y. Tian, B. Cotté, A. Chaigne
UME, ENSTA ParisTech, 828 boulevard des Maréchaux, Palaiseau, France

Summary

Aeroacoustic noise from a wind turbine is mainly caused by the interaction between the wind turbine blade and the air flow. For a modern wind turbine, trailing edge noise is often the dominant noise source. In this paper, a detailed study of trailing edge noise is carried out using Amiet's frequency domain analytical source model. Model results are compared with experimental data. Features of wind turbine noise, such as amplitude modulation, ground directivity, influence of blade twist and pitch are studied. In the last part, the influence of realistic wind profiles is investigated. Wind shear is seen to increase the sound power level and the amplitude modulation.

PACS no. 43.28.Py, 43.28.Ra

1. Introduction

A modern wind turbine converts wind energy into electrical power with satisfying efficiency. The number of wind farms, given the fact that it is a clean and renewable energy, grows very fast in many countries to reduce the reliance on traditional energy sources. Meanwhile, noise from a wind turbine, which is generated aerodynamically is the main concern for the acceptance of wind farms by the neighborhood. The annoyance is enhanced by the amplitude modulation associated with wind turbine noise, that is caused by the rotation of the blade [1].

The main aeroacoustic sources of a wind turbine are the trailing edge noise, the turbulent inflow noise, stall noise and tip noise. Trailing edge noise is caused by the interaction of the boundary layer turbulence with the airfoil trailing edge, and is usually the dominant source for a large wind turbine [2]. The strength of this noise source is influenced by atmospheric conditions, that can be categorized into stable, unstable and neutral. Usually an unstable atmosphere appears in daytime and is characterized by a weak wind shear, while a stable atmosphere is typically present at nighttime with stronger wind shear effects.

In this paper, we focus on wind turbine trailing edge noise, and we adapt Amiet's analytical model to a rotating blade. This paper aims at validating the model against large size wind turbine measurements, at understanding the cause of amplitude modulation, and at investigating the influence of wind profile, blade twist and pitch on the radiated noise. It is organized as follows : in Section 2, Amiet's model is presented and applied to a full size wind turbine. Then, in Section 3, the model is validated by comparing predicted and experimental power spectra, and the effect of twist and pitch are investigated. Finally, calculations with different wind profiles from onsite measurements are carried in Section 4 out to study the influence of atmospheric stability on wind turbine noise.

2. Amiet's analytical model for trailing edge noise

2.1. Presentation of Amiet's analytical model

Amiet's model was first developed for turbulent inflow noise [3], and extended later to trailing edge noise [4]. Figure 1 shows the geometry at the starting point of the model. An incoming flow with a uniform velocity U encounters a flat plate at the leading edge. Turbulence grows inside the boundary layer while convected to the trailing edge, and is scattered at the trailing edge (shown in red in the figure). The plate has a span L and a chord c, and a receiver is located at (x_R, y_R, z_R), where the origin of the coordinate is set at the middle of the trailing edge.
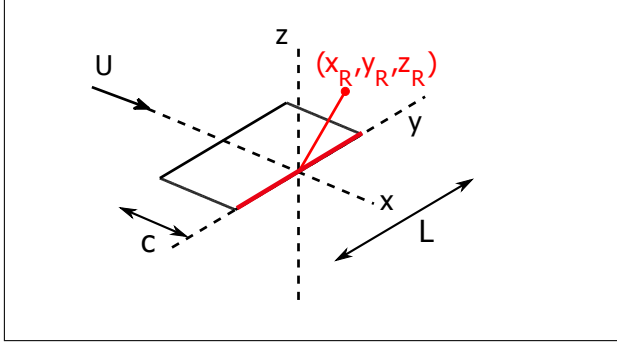
Figure 1. Schematics for Amiet's trailing edge noise model.

Amiet showed that the far field power spectrum density S_{pp} for large aspect ratio can be written as [4] :

$$S_{pp}(x_R, y_R, z_R, \omega) = \left(\frac{\omega c z_R}{4\pi c_0 S_0^2} \right)^2 \frac{L}{2} \left| \mathscr{L} \left(\frac{\omega}{U_c}, \frac{\bar{k}y_R}{S_0} \right) \right|$$
$$\Phi_{pp}(\omega) l_y \left(\omega, \frac{\bar{k}y_R}{S_0} \right), \quad (1)$$

with ω the angular frequency, c_0 the sound speed, S_0 a modified distance between the source and the observer, Φ_{pp} the span-wise wall pressure spectra, l_y the span-wise correlation length, $\bar{k} = kc/2$ the normalized acoustic wavenumber, and $\mathscr{L}$ a transfer function that connects the airfoil surface pressure fluctuation to the acoustic pressure in the far field. Moreau and Roger [5] have shown that the large aspect ratio approximation is valid for $L/c > 1$.
We validated the model for a fixed airfoil in [6]. The main difficulty with the model is to obtain the wall pressure spectra Φ_{pp}. Here we use a scaling law model proposed by Rozenberg *et al.* [7], that considers an adverse pressure gradient flow condition. The span-wise correlation length is estimated using Corcos model [8].

2.2. Model adaption to a rotating blade

Amiet's model was originally developed for a fixed plate. A simplified method to account for the blade rotating motion is to consider a series of discrete angular positions. Blandeau showed that this approximation is valid within a given range of frequencies [9]. Trailing edge noise varies along the blade due to the variations of turbulence parameters, wind speed and blade geometry, thus it is necessary to divide the long blade into short segments in order to describe these variations. However, another limitation on the segment length is that it has to be larger than the span-wise wall pressure correlation length l_y, so that two neighboring segments can be assumed uncorrelated. Once the number and size of the blade segments has been chosen, the noise is calculated according to the following steps :
1. launch XFOIL to calculate the boundary layer parameters required by the wall pressure model;

Table I. Parameters for the 3 test cases

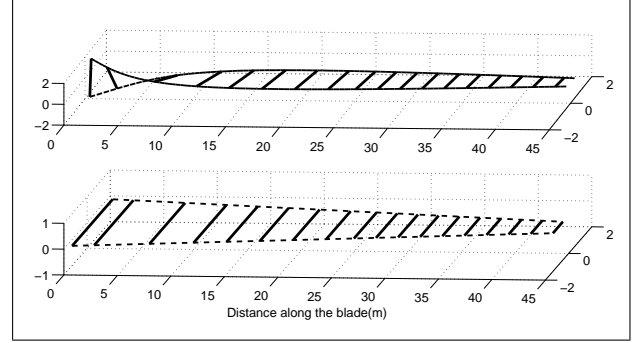|	Wind speed (m/s)	Rotor speed (rpm)	Pitch (^{o})
case 1	6	13	3
case 2	8	14	-2
case 3	9.5	17	5

Figure 2. Geometry of a blade of 45 m length with twist (top) and without twist (bottom).

2. use Amiet's model to calculate the far field pressure spectrum S_{pp} for each segment at a certain blade position;
3. apply Doppler correction and calculate the total noise spectrum by logarithmic summation;
4. move to the next blade position and repeat the step 1 and 3.

3. Application on a wind turbine

3.1. Configuration studied

The model wind turbine is a 2.3 MW Siemens SWT 2.3-93. The tower height (ground to hub) is 80 m, the blade length is 45 m and it has 3 blades that have controllable pitch angle. The chord length is 3.5 m at the root of a blade, and 0.8 m at the tip. A linear variation is assumed as shown in Figure 3. These data in addition to the measurements are found in [10]. Three cases mentioned in this reference are summarized in Table I. In this paper, only the results from case 2 and case 3 are presented. A constant wind profile (no shear) is considered in this section.

Pitch angle is applied by rotating the blade around the blade axis as a whole. It changes the angle of attack (AoA) by the same amount for all the segments. Here, by default, a positive pitch decreases AoA while a negative pitch increases AoA. The blade twist is chosen so that the AoA is 7° by default. An illustration of a twisted blade is shown in Figure 2.

Before the calculation, it is needed to decide how to divide the blades. The largest wind speed provided in [10] is 9.5 m/s, thus the largest span-wise correlation
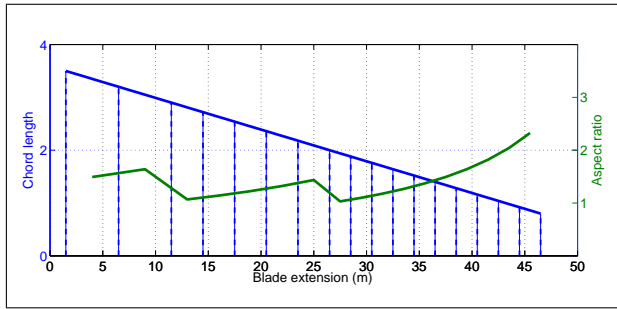
Figure 3. Chord length (blue) and aspect ratio (green) of each segment. The vertical blue lines indicate the 17 segments.
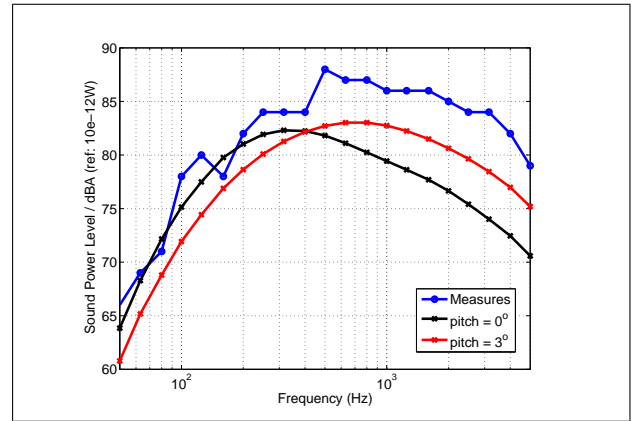

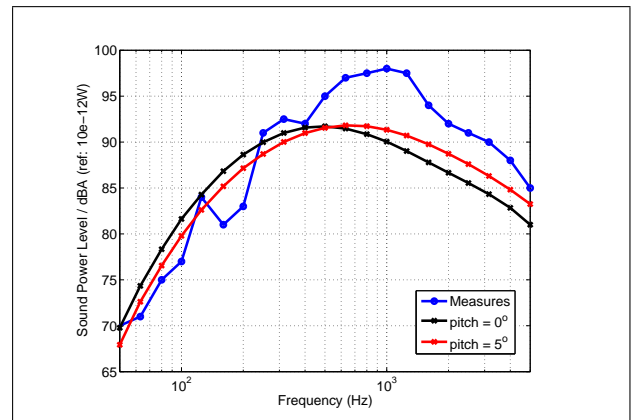Figure 4. Sound power level spectra for case 1.

Figure 5. Sound power level spectra for case 3.

Figure 6. Sound power level spectra for different pitch angle settings with a constant wind speed of $9.5\,m/s$.

length is less than 0.5 m according to Corcos model. In this study, we propose to divide the blade into 17 segments, whose length ranges from 5 m to 2 m from the root to the tip. The aspect ratio for each segment is shown in Figure 3, and remains greater than unity.

3.2. Sound power level calculations and comparison to measurements

The third octave band spectrum of the sound power level L_W is calculated from the sound pressure level at a receiver 100 m downwind of the wind turbine; the spectra are averaged over a complete rotation. Measured and calculated spectra are compared in Figures 4 and 5 for cases 1 and 3, respectively. The results agree well for frequencies below 400-500Hz, and increases with increasing constant wind speed. We also notice that the pitch angle changes the shape as well as the peak frequency of the spectra. For $U = 6m/s$, results considering pitch fit better over the whole frequency range. For $U = 9.5m/s$, the pitch-included spectrum has a shape closer to the measured one. However, there are discrepancies for both cases, which can be attributed to other noise sources that are not taken into account in the calculations, and to the atmospheric conditions during the measurements that could differ from the constant wind profile considered here.

Figures 4 and 5 show that the pitch angle has an influence on the shape of the spectrum. The reason is that the pitch angle changes the AoA at leading edge, thus changing the surface pressure fluctuations inside the boundary layer. In Amiet's model, the radiated noise spectrum is determined by the surface wall pressure spectrum, so the change of wall pressure inside the boundary layer modifies the radiated noise. Figure 6 shows the influence of the pitch angle for $U = 9.5\,m/s$ case. Along with increasing pitch angle (thus decreasing AoA), the peak frequency moves to the right, and the maximum L_W increased, except for a pitch of 5°.

3.3. Amplitude modulation and directivity

Amplitude modulation is caused by the rotation of the blades. It has a frequency of $1/3$ of the blade rotating frequency. In Figure 7, the relative variations of sound pressure level are shown for two observer locations. The variations can reach up to 8 dB for a crosswind observer, while it is almost constant for a downwind direction. Figure 8 shows the directiv-
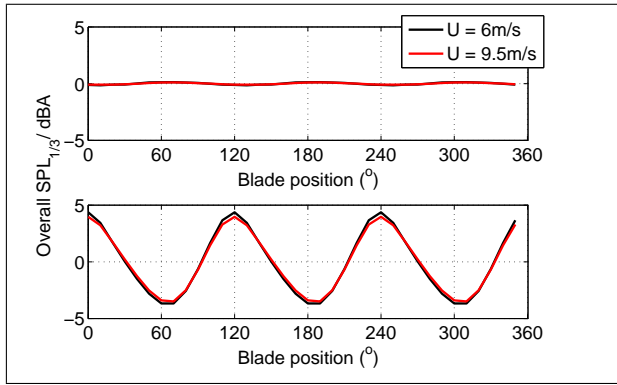
Figure 7. Amplitude modulation in wind direction (top) and cross-wind direction (bottom). The observer is 100 m away from the wind turbine in the two directions. The results are subtracted from the mean sound pressure level.
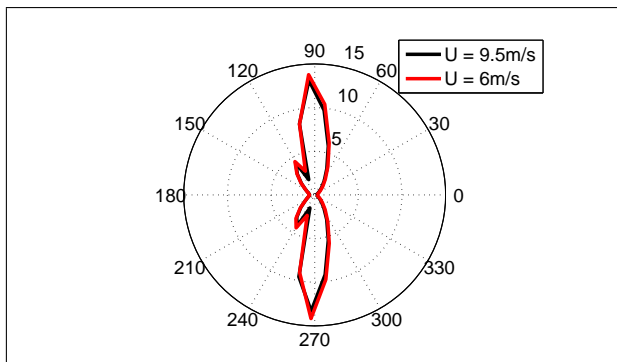
Figure 8. Directivity of amplitude modulation strength in dB, at a distance of 100 m away from the wind turbine.
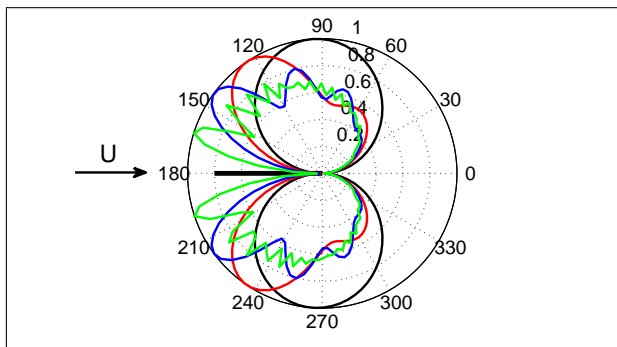
Figure 9. Directivity of trailing edge noise predicted by Amiet's model at 16 Hz (black), 50 Hz (red), 120 Hz (blue) and 500 Hz (green). The flat plate is represented in black.

ity of amplitude modulation strength for cases 1 and 2. We can see that the strongest amplitude modulation appears in the direction a little upwind from the rotor plane, while the overall directivity pattern does not vary a lot with different wind speeds.

Amiet's model assumes that the surface pressure fluctuations along the blade radiate in a dipole-like fashion. The directivity of trailing edge noise is thus determined by the orientation of the plate, and
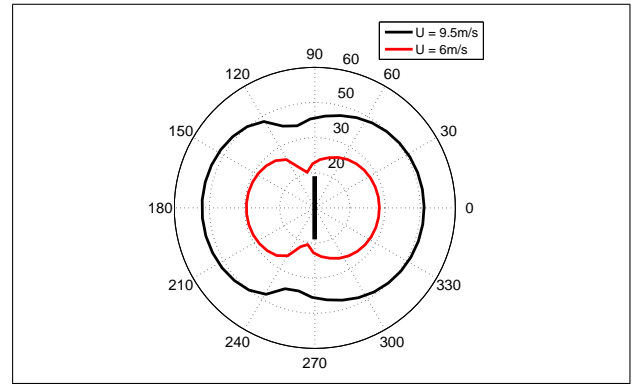
Figure 10. Directivity plot of overall SPL in dB(A). The black line indicates the rotor plane when looking from above. The wind is coming from the left.

depends on frequency as seen in Figure 9. Considering blade twist, the orientation of the dipole will change along the blade, which explains that the horizontal directivity plot obtained in Figure 10 loses the typical dipole pattern that was shown in [6]. The minimum overall sound pressure level (SPL) moved to the direction slightly upwind from the rotor plane where the maximum amplitude modulation was found.

4. Atmospheric condition impact on the trailing edge noise

4.1. Wind profiles obtained by SIRTA data

In reality, wind turbines are always working in an atmosphere where the wind is turbulent and nonuniform. Our goal is to know how the realistic wind profile impacts the generated noise. The SIRTA (Site Instrumental de Recherche par Télédétection Atmosphérique) is an atmospheric observatory located 20 km south of Paris [11]. An anemometer provides 10 min averaged wind speed at 10 m height, as well as the averaged wind direction. A Doppler lidar measures the wind speed profile between 40 m and 200 m height. In addition, a sonic anemometer measures the wind fluctuations which allow us to estimate the friction velocity u_*, and temperature scale T^*. Monin-Obukhov similarity theory (MOST) is used to obtain the wind profile in the vertical direction. Atmospheric conditions can be classified by the Obukhov length scale L^*, which is related to u_* and T^*:

$$L^* = \bar{T} \, u_*^2/(\kappa g T^*), \qquad (2)$$

where $\bar{T}$ is the mean temperature potential, κ is the von Kármán constant, and g is the gravity. A physical interpretation of L^* can be given as the height at which the buoyant production of turbulence kinetic energy is equal to the wind shear production.
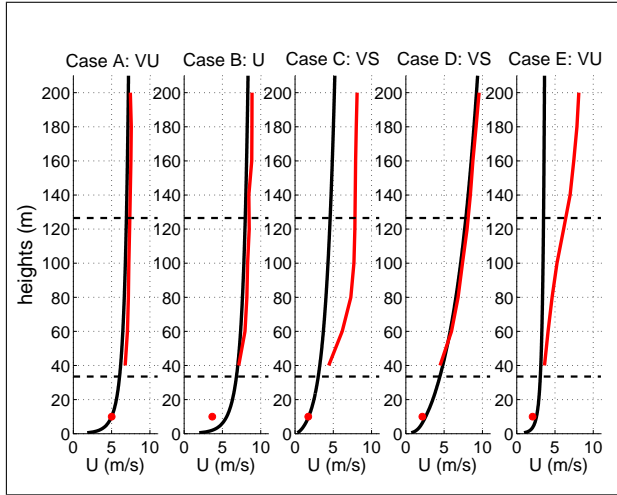
Figure 11. Wind profiles calculated by MOST (black line) compared to SIRTA data (red line). Red marker stands for the 10 min averaged wind speed at 10 m height. The two horizontal dash lines correspond to the lowest and highest altitude that a blade can reach.

Table II. Atmospheric conditions for 5 chosen periods.

	$U_{hub}(m/s)$ Lidar	$U_{hub}(m/s)$ MOST	u_* m/s	T^* K	L^* m
case A	7.2	6.7	0.47	-0.11	-141
case B	8.2	7.6	0.51	-0.05	-330
case C	7.3	4.0	0.06	0.05	5.7
case D	6.8	6.5	0.17	0.07	32
case E	4.6	3.4	0.25	-0.05	-84

To obtain realistic wind profiles, measurements from SIRTA are analyzed for a chosen day (a period of 24 h) when the wind was mostly from the west where the terrain is open and flat. Vertical wind profiles obtained by MOST for 5 chosen durations within 24 h are shown in Figure 11. Corresponding friction velocities, temperature scales and Obukhov length scales obtained from the measurements as well as by MOST are listed in Table II. There are limitations for MOST, as we can see that for some periods MOST profiles do not fit the measurements. The following results will only focus on very unstable case A and very stable case D .

4.2. Effects of wind shear on sound power spectra

The calculated sound power level spectra for cases A and D are shown in Figures 12 and 13, and compared to the results for a constant wind speed profile equal to the wind speed at hub height (80 m). For case A, the wind profile has really weak shear, representing an unstable atmosphere, and only slight differences at high frequencies are observed. For case D, the measured wind profile has strong shear, which indicates
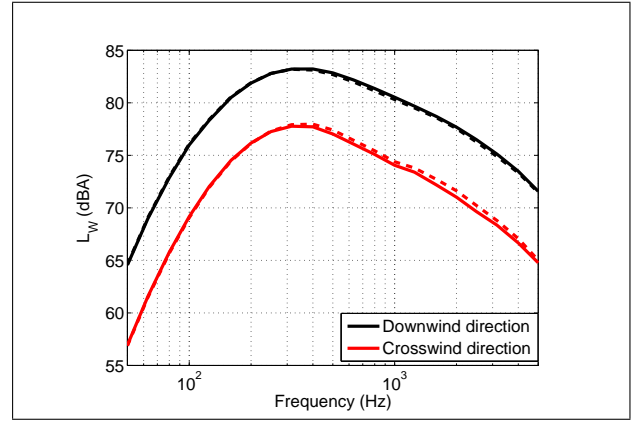

Figure 12. Sound power level of case A. Solid: wind profile with shear; dash: constant wind profile
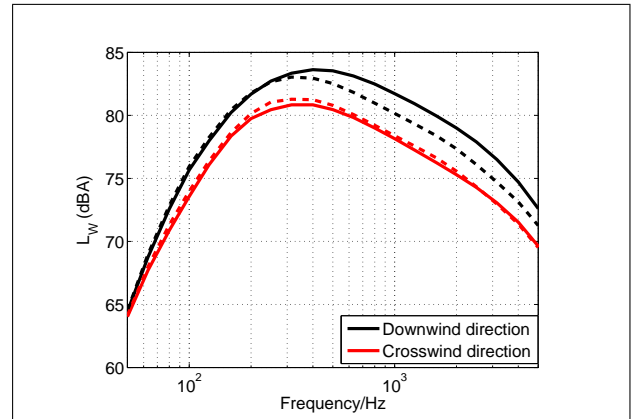

Figure 13. Sound power level of case D. Solid: wind profile with shear; dash: constant wind profile

a stable atmosphere, and an increase of L_W of 2 dB at high frequencies is observed in the downwind direction. L_W in the crosswind direction is only weakly influenced by the wind shear.

4.3. Effects of wind shear on directivity and amplitude modulation

The normalized overall SPL and the normalized amplitude modulation strength are plotted in Figure 14 as a function of the ground azimuthal angle τ. The results are shown in relative dB by subtracting the minimum value from the maximum during one rotation. We can see that due to the blade twist effect, the minimum overall sound pressure level is no longer at crosswind direction, where the strongest amplitude modulation is found. At τ around 100°, the overall sound pressure reaches a minimum, while the amplitude modulation strength is only half the maximum value. Also it is shown in the figure that the crosswind direction amplitude modulation is stronger on the side where the blades rotate downwards ($\tau = 270^o$) than on the one where the blades rotate upwards ($\tau = 90^o$).
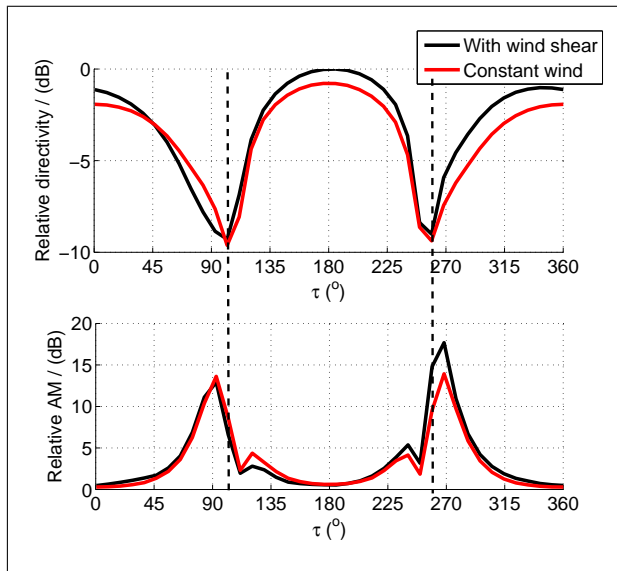
Figure 14. Normalized overall SPL (top) and normalized amplitude modulation strength (bottom) with respect to ground azimuthal angle τ.
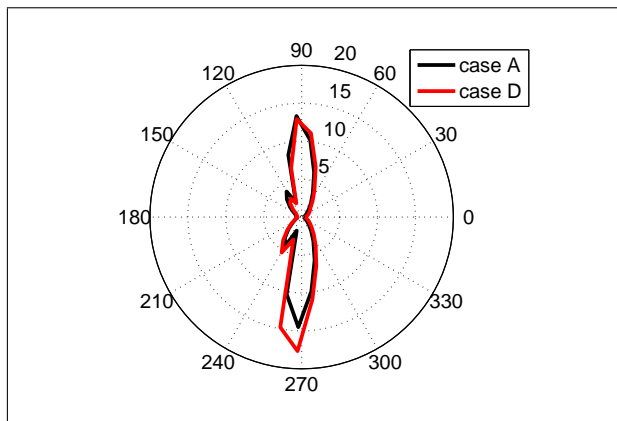

Figure 15. Directivity of amplitude modulation strength for cases A and D.

The directivity of amplitude modulation strength for cases A and D are plotted in Figure 15. For $\tau = 270^o$ direction, where the blades rotate downwards, the amplitude modulation is stronger when the strong wind shear of case D is present.

5. Conclusions and perspectives

In this study, Amiet's analytical model for trailing edge noise is applied for wind turbine noise prediction. The trailing edge noise spectrum is determined from the surface pressure fluctuation. Since the twist angle and the pitch angle change the AoA at the leading edge, surface pressure at the trailing edge is modified. Twist and pitch angle also have an influence on the ground directivity. When the blade twist is considered, the ground directivity loses the typical dipole shape. Wind shear increases the trailing edge

noise, especially in the wind direction. The increase is most noticeable at frequencies higher than the peak frequency. From the results, wind shear increases the amplitude modulation in the crosswind direction where the blades rotate downwards ($\tau = 270^o$). With blade twist, the minimum directivity is not exactly in the crosswind direction where amplitude modulation is the most significant, meaning that in the direction where the minimum noise is perceived (in case D $\tau = 100^o$ and 260°), the amplitude modulation strength is only half the maximum value.

In the future, we will study the effect of atmospheric variability on wind turbine noise, and the influence of the orientation of the rotor plane with respect to the wind direction. Also, other noise sources such as turbulent inflow noise will be investigated.

References

[1] V. V. Lenchine: Amplitude modulation in wind turbine noise. Proc of ACOUSTICS 2009 Nov. Australia.

[2] S. Oerlemans, J. G. Schepers: Prediction of wind turbine noise and validation against experiment. International Journal of Aeroacoustics, Aug 2009, pp. 555-584.

[3] R.K. Amiet: Acoustic Radiation from an Airfoil in a Turbulent Stream, Journal of Sound and Vibration, 1975, Vol 41, pp 407-402.

[4] R.K. Amiet: Noise Due to Turbulent Flow Past a Trailing Edge, Journal of Sound and Vibration, 1976, Vol.47, pp 387-393.

[5] S. Moreau, M. Roger: Back-scattering correction and further extensions of Amiet's trailing-edge noise model. Part II: Application. Journal of Sound and Vibration. Vol 323 (2009), pp. 397-425.

[6] Y. Tian, B. Cotté, A. Chaigne, *Wind turbine noise modeling based on Amiet's theory*, 5th Wind Turbine Noise Conference, Denver, USA, 28-30 August (2013).

[7] Y. Rozenberg, G. Robert, S. Moreau, Wall-pressure spectral model including the adverse pressure gradient effects, AIAA Journal **50**(10), 2168-2179 (2012).

[8] G. M. Corcos: Resolution of pressure in turbulence, J. Acoust. Soc. Am. 1963. Vol.35, no.2, pp. 192-199.

[9] V. P. Blandeau, P. F. Joseph: Validation of Amiet's model for propeller trailing-edge noise. AIAA Journal, Vol. 49, no. 5, 2011.

[10] G. Leloudas, Optimization of wind turbines with respect to noise, Master thesis DTU (2006).

[11] M. Haeffelin *et al.*, SIRTA, a ground-based atmospheric observatory for cloud and aerosol research, *Annales Geophysicae* **23**, 1-23 (2005).